ADVANCES IN NUCLEAR SCIENCE AND APPLICATIONS

Volume 1, No. 1 (2025), P. 05-16

Quasifission process in the reactions of ^{48}Ca ions with deformed nuclei

G.N. Knyazheva*[,1,2], E.M. Kozulin[1,2], A.A. Bogachev[1], I.M. Itkis[1], M.G. Itkis[1]

[1]Joint Institute for Nuclear Research, Dubna, Russia

[2]Dubna State University, Dubna, Russia

e-mail: knyazheva@jinr.ru

Received: 10 February 2025

Abstract

The study of orientation effects in the interactions of ^{48}Ca ions with well deformed nuclei is presented. Two cases are considered, namely, the reactions with actinides leading to the formation of superheavy systems, as well as with lanthanides in which less fissile composite systems in the region of Hg–Pa are formed. The properties of mass and energy distributions of quasifission fragments originated in these reactions are discussed.

Introduction

At present the heaviest nuclei up to $Z = 118$ have been produced in the complete fusion reactions of ^{48}Ca ions with actinide targets [1]. ^{48}Ca plays a key role in this success due to it exotic structure. It is a doubly magic nucleus ($Z = 20$, $N = 28$) consisting of ^{40}Ca core and a neutron skin. Neutron skin permits to increase the nuclear attraction and reduce the Coulomb repulsion at the reaction contact point that creates favorable conditions for formation of compound nucleus (CN) in further evolution of composite system. Moreover, additional 8 neutrons give a possibility to form more neutron-rich superheavy nuclei (SHN) located much close to the predicted *island of stability*.

The Coulomb factor Z_1Z_2 (charge product of reaction partners) is one of the main parameters that determines the interaction mechanism of two massive nuclei:

CN formation, quasifission (QF) or deep inelastic collisions (DICs). Quasifission [2-7] and deep inelastic collisions [8-10] are binary multinucleon transfer reactions with a full momentum transfer in which the composite system separates in two main fragments without forming a CN. QF happens to be the most important mechanism that prevents the formation of superheavy elements in the fusion of heavy nuclei. The ratio between QF and CN formation is mainly determined by the entrance channel properties [2-7]. Generally, one use three experimental criteria to identify the reaction mechanism (fusion or QF), namely, the reaction Coulomb factor Z_1Z_2 [11], entrance-channel mass asymmetry $\alpha_0 = |A_{\text{target}} - A_{\text{projectile}}|/A_{\text{CN}}$ [12], and the mean fissility parameter $x_m = 0.75x_{\text{eff}} + 0.25x_{\text{CN}}$ [13].

After capture of interacting nuclei, to form evaporation residues (ER) a composite system has to overcome QF, to fuse to an equilibrated CN and to survive against fission during deexcitation process. Experimentally, the capture cross section is defined as the sum of the QF, CN-fission and ER cross sections. The fusion probability PCN is defined as the probability of CN formation after capture and depends strongly on the reaction entrance channel properties, such as Z_1Z_2, α_0, x_m, interaction energy, deformation of reaction partners etc., whereas the CN survival probability depends only on the fission barrier, excitation energy and angular momentum of formed CN. The predicted fission barriers for SHN are about 3-10 MeV [14-17]. Due to the high fissility of SHN caused by the relatively small fission barrier only a minor part of the CN-formation cross section is expected to fall into the ER channel. The excited CN formed in fusion reaction mainly undergoes fission. The study of fission of heavy and superheavy nuclei gives important information about the CN-formation cross section, the fission barriers and survival probabilities of these nuclei.

It is known that static deformation of the interacting nuclei also affects the reaction mechanism. The orientation effect was found experimentally in the reactions with well deformed nuclei [18, 19]. The different orientations of deformed nuclei at the contact point cause the changes in the balance between the Coulomb and nuclear forces and, as a result, vary the further evolution of formed composite system. A high CN-formation probability is expected for the compact collisions (side-to-side), whereas the elongated configuration (tip-to-tip) is favorable for QF. The driving potentials for the $^{48}\text{Ca} + ^{248}\text{Cm}$ system for compact and elongated configurations calculated by V. Zagrebaev [20] are shown in Figure 1. Notice that for the compact collision the Coulomb barrier in the entrance channel is significantly higher. Nevertheless, as seen in the figure due to the compact configuration the path to CN formation is much shorter comparing to the elongated collision. Thus, one may expect higher fusion probability for compact collision.

In the superheavy element synthesis experiments the actinide target materials (natural and artificial) were used. The actinides are well deformed nuclei with $\beta_2 \approx 0.2 - 0.3$. Most of the lanthanides except the nuclei around neutron shell at $N = 82$ are also well deformed. Thus, we may expect the manifestation of orientation effects in the reactions of Ca ions with actinide and lanthanide nuclei. Note that in the case of lanthanides the criteria given above are favorable to CN formation, while for actinides – to QF process.

This work is devoted to the study of orientation effects in superheavy composite systems as well as in less fissile composite systems in the Pb–Th region. The properties of binary fragments formed in the reactions of $^{40,48}\text{Ca}$ with $^{144,154}\text{Sm}$, ^{168}Er, ^{238}U, and $^{48}\text{Ca} + ^{244}\text{Pu}$, ^{248}Cm are discussed. Special attention is paid

to the $^{48}\mathrm{Ca} + ^{154}\mathrm{Sm}$, $^{238}\mathrm{U}$ reactions for which a detailed experimental study of capture cross sections, mass-energy distributions of binary reaction fragments [19, 21] together with experimentally measured ER cross sections [22, 23] at energies near the Coulomb barrier was performed. The entrance channel parameters of the studied reactions are presented in Table I.

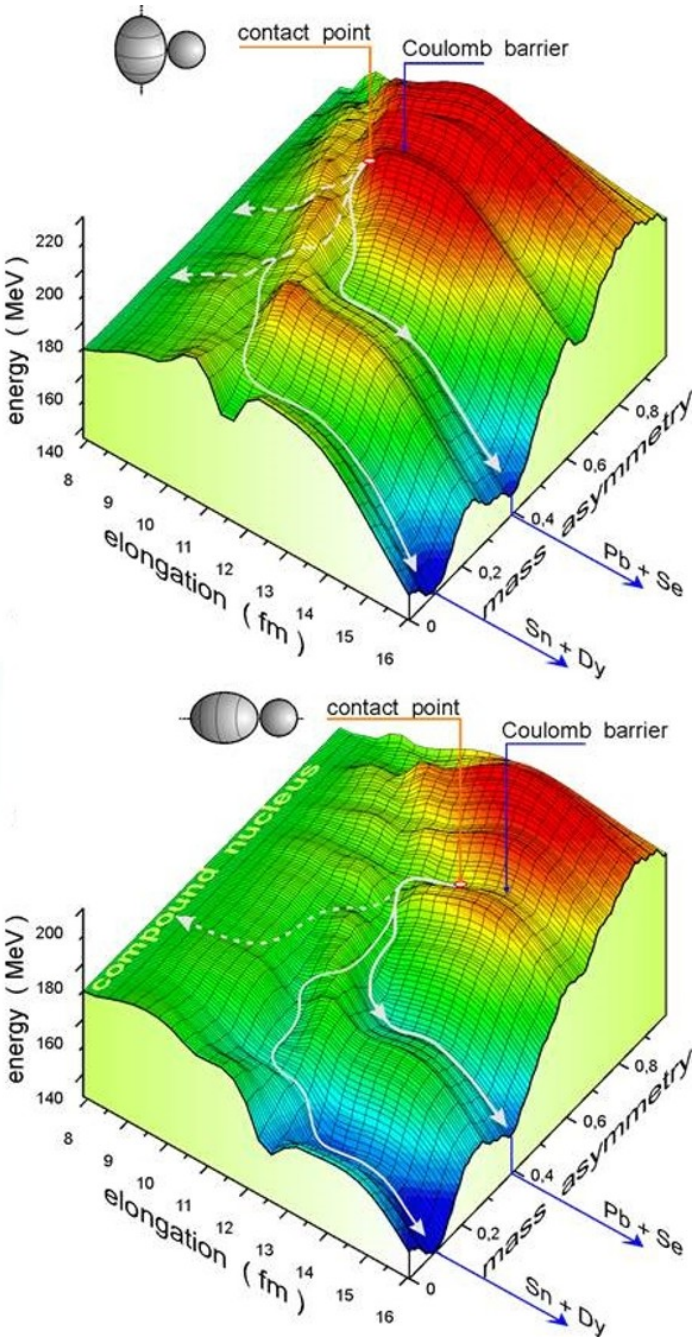

Figure 1: The driving potentials in the space of mass asymmetry and elongation for the $^{48}\mathrm{Ca} + ^{248}\mathrm{Cm}$ reaction for compact (top panel) and elongated (bottom panel) configurations calculated by V. I. Zagrebaev (from Ref. [20]).

Table 1: The reaction entrance channel properties for the systems under study: the charge product of interacting nuclei Z_1Z_2, entrance-channel mass asymmetry α_0, mean fissility parameter x_m and β_2 deformation of the target nuclei.

Reaction	Z_1Z_2	α_0	x_m	β_2
^{48}Ca+^{144}Sm	1240	0.500	0.628	0.0
^{48}Ca+^{154}Sm	1240	0.525	0.620	0.270
^{48}Ca+^{168}Er	1360	0.556	0.653	0.297
^{48}Ca+^{238}U	1840	0.664	0.770	0.236

1 QF in the reactions of ^{48}Ca ions with lanthanides

For the first time, the appearance of quasi-fission (QF) in the reactions of Ca ions with lanthanides was observed in Ref. [24]. The mass and energy distributions of binary fragments formed in the $^{12}\mathrm{C}+^{204}\mathrm{Pb}$ and $^{48}\mathrm{Ca}+^{168}\mathrm{Er}$ reactions leading to the same compound nucleus $^{216}\mathrm{Ra}^*$ at the excitation energy of 40 MeV were measured using the double-arm time-of-flight CORSET setup [25]. The mass-energy distributions from Ref. [24] are presented in Figure 2. The distributions for the $^{12}\mathrm{C}+^{204}\mathrm{Pb}$ reaction are well described by the liquid drop model (LDM), namely, the mass distribution has a Gaussian shape, and the average total kinetic energy (TKE) has a parabolic dependence on fragment mass. A small amount (1.5%) of asymmetric fission is found.

Contrary to $^{12}\mathrm{C}+^{204}\mathrm{Pb}$, the mass yield of fragments formed in the $^{48}\mathrm{Ca}+^{168}\mathrm{Er}$ reaction differs significantly from LDM prediction in the region of asymmetric fragments. The average TKE in this case is about 10-15 MeV higher than the expected LDM value. The contribution of asymmetric fission is about 30%. This marked increase in the yield of asymmetric products is connected to the QF. In the mass distribution for $^{48}\mathrm{Ca}+^{168}\mathrm{Er}$ [see Figure 2 (d)] the position of closed proton and neutron shells at Z = 28, 50 and $N = 82$ calculated in the assumption of unchanged charge density [26] are shown by arrows. It is seen that the major part of QF fragments is concentrated near the shells $Z = 28$ and $N = 82$ that indicates the importance of shell effects in the formation of QF fragments for this system.

Despite the fact that ^{168}Er is a well deformed nucleus no direct indication of the impact of orientation effect on QF process was found. The entrance channel properties vary strongly for these two reactions. The charge product Z_1Z_2 increases by a factor of 2.7. Possibly it plays a crucial role in the reaction dynamics for these nuclear systems.

The answer on a question about the reason of QF appearance for such systems was obtained from the measurements of mass-energy distributions of fragments formed in the $^{48}\mathrm{Ca}+^{144,154}\mathrm{Sm}$ reactions [19]. These reactions have a similar entrance channel properties (see Table I) and based on the reaction mechanism criteria the contribution of QF process is expected to be similar. However, ^{144}Sm is a spherical nucleus, whereas ^{154}Sm is well deformed.

The mass distributions of fissionlike fragments formed in the $^{48}\mathrm{Ca}+^{144,154}\mathrm{Sm}$ reactions at the Coulomb barrier energies measured using the CORSET setup [25] are shown in Figure 3. Similarly to the $^{48}\mathrm{Ca}+^{168}\mathrm{Er}$ system, the QF asymmetric

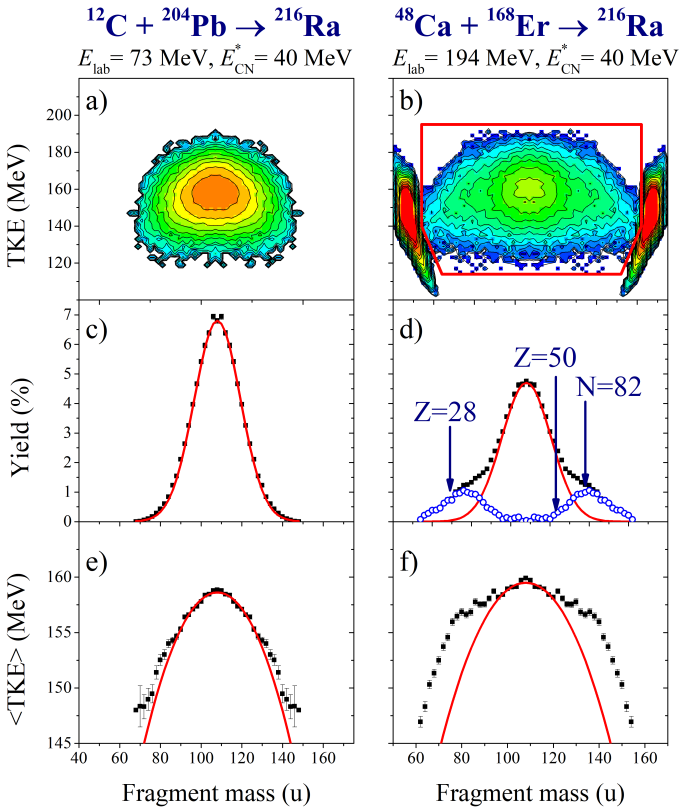

Figure 2: Mass-energy distributions of fragments formed in the $^{12}\mathrm{C}+^{204}\mathrm{Pb}$ (a) and $^{48}\mathrm{Ca}+^{168}\mathrm{Er}$ (b) reactions. The mass yields (c)–(d) and average TKE as a function of fragment mass (e)–(f) for the events located inside the red contour on MTKE matrix in the case of the $^{48}\mathrm{Ca}+^{168}\mathrm{Er}$ reaction. Solid lines are LDM calculations.

fragments are found for the reaction with well deformed ^{154}Sm. The angular distributions for these fragments also measured in [19] show the pronounced forward-backward asymmetry that proves their QF origin. In the case of the $^{48}\mathrm{Ca}+^{144}\mathrm{Sm}$ reaction the asymmetric QF fragments were not observed in the mass distribution and mass-angular distributions agree well with expectation for CN fission as for symmetric as well as for asymmetric fragments.

The relative contribution of QF into the capture cross section (the sum of ER, CN-fission, and QF cross sections) for the $^{48}\mathrm{Ca}+^{154}\mathrm{Sm}$ reaction is shown in Figure 4. One can see that at low energies, the fraction of QF is around 20% of capture cross section. However, at higher energies, it becomes smaller. In the simplest prescription proposed by D.J. Hinde in Ref. [18] to explain the anomalous large anisotropy found for the $^{16}\mathrm{O}+^{238}\mathrm{U}$ system by the presence of QF process, the composite system is assumed to fuse if the angle between the separation vector and the symmetry axis of the deformed nucleus exceeds a certain value. This of course means that the interaction energy has to exceed a certain value. This is, however, somewhat extreme. To solve this problem, N. Rowley proposed to use the spirit of the compactness concept with a more general parametrization of probability of QF PQF with the Fermi-function form [27]:

$$P_{\mathrm{QF}} = \gamma_{\mathrm{QF}} \frac{1}{1+\exp\left(\frac{B_\alpha - B_{\mathrm{QF}}}{\Delta_{\mathrm{QF}}}\right)}, \tag{1}$$

where γ_{QF} is a fraction of QF for the non-compact barriers, reducing to zero for the

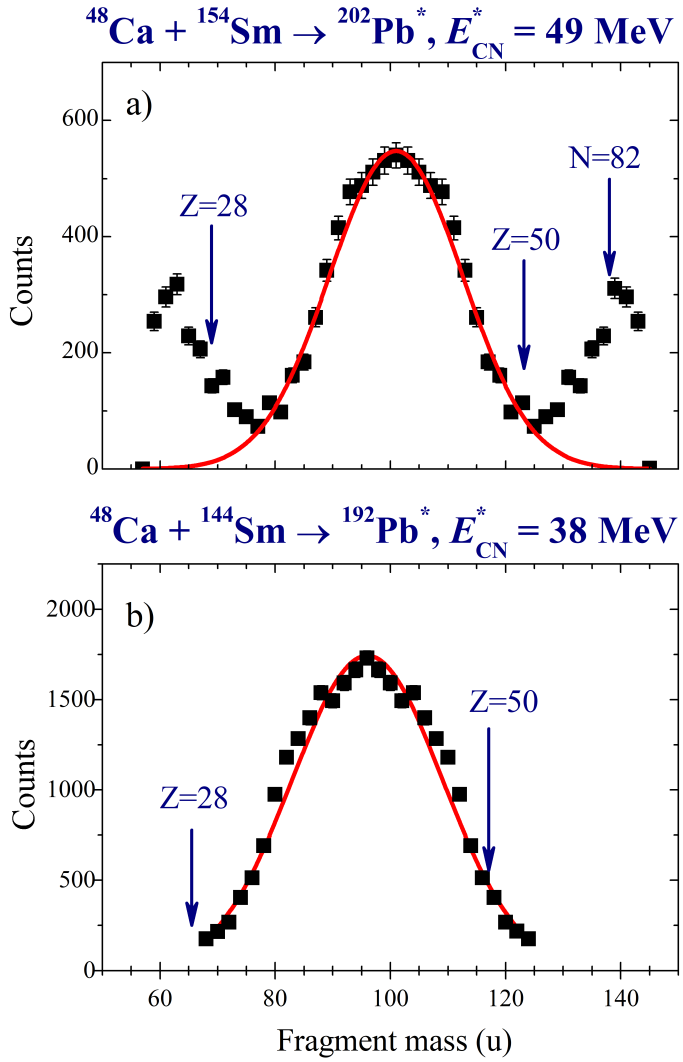

Figure 3: Mass distributions of fissionlike fragments formed in the $^{48}\mathrm{Ca} + ^{144,154}\mathrm{Sm}$ reactions at the Coulomb barrier energies. Solid lines are LDM calculations. Arrows indicate the position of closed proton and neutron shells.

more compact ones. For $^{48}\mathrm{Ca} + ^{154}\mathrm{Sm}$ $\gamma_{\mathrm{QF}} = 0.2$, $B_{\mathrm{QF}} = 138.5$ MeV, $\Delta_{\mathrm{QF}} = 1$ MeV. The parameters B_{QF} and Δ_{QF} describe the way that the QF is cut off for the compact barriers [dashed curve in Figure 5 (a)] which proceed essentially to CN creation. Capture barrier distributions obtained from experimental capture cross section in [22] and the result of CCFull calculation for capture barrier distribution [27] together with the part of this distribution which contributes to QF for the $^{48}\mathrm{Ca} + ^{154}\mathrm{Sm}$ calculated via proposed PQF are presented in Figure 5 (a).

Then the QF cross sections may be calculated as [27]:

$$\sigma_{\mathrm{QF}}(E_{\mathrm{c.m.}}) = \frac{\pi}{k^2} \sum_{l,\alpha} (2l+1)\, \omega_\alpha T_l(E, B_\alpha) P_{QF}(E_{\mathrm{c.m.}}) \qquad (2)$$

The measured capture, QF, CN-fission and ER cross sections for $^{48}\mathrm{Ca} + ^{154}\mathrm{Sm}$ in [19] are shown in Figure 5 (b) together with N. Rowley calculations performed using the expressions given above. It is seen from the figure that in such approach the experimental cross sections can be well described for all possible reaction channels for the studied system. The data may certainly be said to require around 20% QF

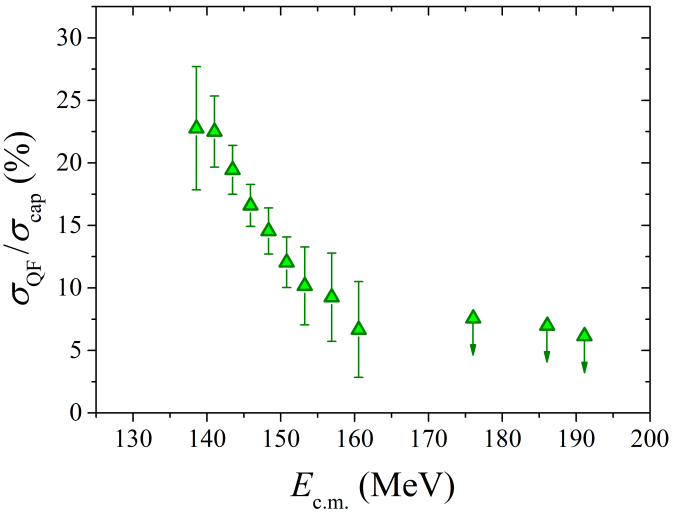

Figure 4: The experimentally extracted contribution of QF component into the capture cross sections in the $^{48}Ca + ^{154}Sm$ reaction in dependence on the interaction energy (from Ref. [19]).

for the low barriers and very little from the highest ones, confirming the presence of orientation effect in this system.

Thus, the orientation effect in the reactions of Ca ions with well deformed lanthanide nuclei leads to appearance of QF fragments. In this case the QF mass distributions are asymmetric. The heavy QF fragments formed in such systems are peaked around the heavy mass 140 u near the neutron shell at $N = 82$.

2 QF in the reactions of ^{48}Ca ions with actinides

Theoretical calculations for such reaction type [28, 29] showed that there are two deep valleys on the potential energy surface of superheavy composite systems, caused by the influence of shell effects (see Figure 1). These valleys are associated with the formation of doubly magic lead ($Z = 82$, $N = 126$) and tin ($Z = 50$, $N = 82$) in the exit reaction channel and lead to appearance of two distinct quasifission processes with different time scales, namely, the first and second types of quasifission (QF I and QF II, respectively).

The experimental study of heavy-ion collisions proves the existence of QF I and QF II [21, 30]. It is known that in superheavy composite systems QF I mainly leads to the formation of asymmetric fragments with mass asymmetry of ~ 0.4 characterized by asymmetric angular distributions in the center-of-mass (c.m.) system and thus fast reaction times ($\sim$ 10-21 sec.) [3]. The TKE for these fragments is higher than that for CN-fission ones [31] and hence this process is colder than CN fission. Due to this reason shell effects in QF are more pronounced. QF II process is characterized by longer reaction times sufficient for mass equilibration and resulting in the formation of symmetric fragments. The angular distribution of these fragments is symmetric with respect to 90° in the c.m. system and the estimated reaction time is about 10-20 sec. typical for CN fission [3].

Experimental mass-angle distributions of QF fragments formed in $^{48}Ca + ^{238}U$ were measured and interpreted using time dependent Hartree-Fock (TDHF) calculations in [32]. It was found that at the interaction energies below and near the

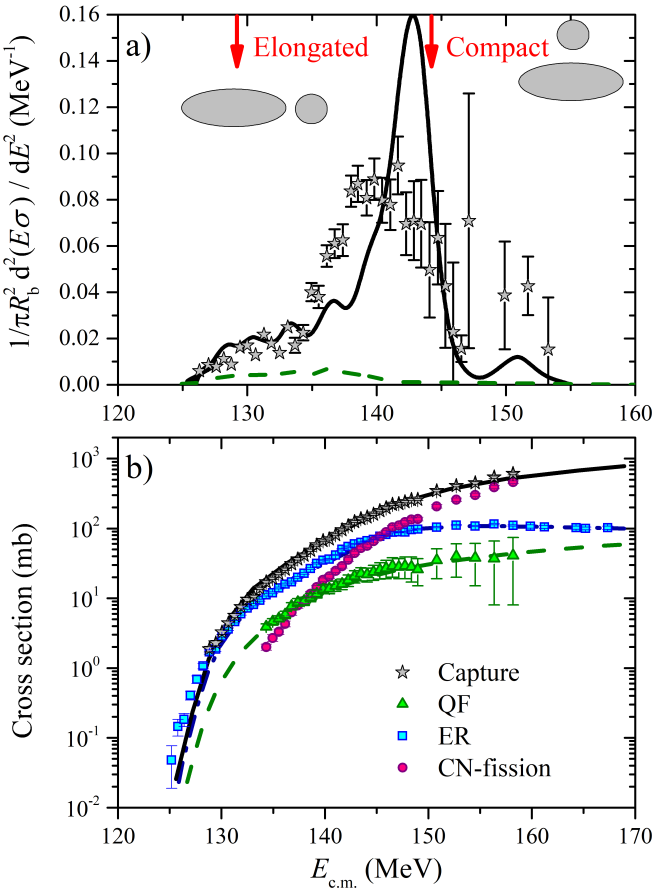

Figure 5: (a) Capture barrier distribution obtained from experimental capture cross section in [22] for the ^{48}Ca + ^{154}Sm reaction (stars). The solid line is the result of CCFull calculation of capture barrier distribution for 48Ca+154Sm from Ref. [27], the dashed curve is the part of this distribution which contributes to QF of the CC calculations (see Ref. [27] for details). The arrows indicate the position of the interacting barriers for compact and elongated configurations. (b) The CN-fission, ER, QF and capture sections measured for ^{48}Ca + ^{154}Sm from [19]. Lines are the QF, ER and capture cross sections calculated using the barrier distribution shown in panel (a).

Coulomb barrier the QF I is a dominant process leading to the formation of fragments with the mass ratio of about 0.25 and 0.75. According to TDHF calculations this asymmetric quasifission is related to shell effects in the $Z \sim 82$ region and occurs in the ^{238}U tip collisions (elongated configuration), leading to short quasifission times. At the energy above the barrier ($E_{c.m.}/E_B = 1.142$), formation of symmetric fragments becomes dominant. No quantum shell effects were predicted by TDHF in the ^{238}U side collisions (compact configuration). Long contact times compatible with fusion are found only for this orientation.

The comparative study of mass distributions for the ^{48}Ca + ^{238}U and ^{40}Ca + ^{238}U reactions measured in [33] shows a good agreement between the shapes of the mass distributions, when the incident energies ($E_{c.m.}$) are the same. Generally, the yield and properties of QF fragments strongly depend on the interaction energy above the barrier ($E_{c.m.}/E_B$).

The mass-energy distributions of the binary fragments formed in the ^{48}Ca + ^{238}U

reaction were measured using the CORSET setup at energies below and above the Coulomb barrier [21]. The M-TKE distributions and the mass yields for fissionlike fragments (events inside the red contour lines in M-TKE matrices) from [21] are shown in Figure 6. The TKE distributions of symmetric fission-like fragments with masses $A\mathrm{CN}/2 \pm 20$ u are also presented in the figure. The TKE distributions have a complex structure which is not consistent with only CN fission. In fact, it is known that in such a case the TKE distribution shows a typical Gaussian-like shape with an average value substantially independent on the excitation energy [4]. This three-hump structure manifests itself at all measured energies. It is important to note that the middle hump corresponds to CN-fission expectation for the ^{286}Cn compound nucleus fission.

It was assumed in [21] that the low-energy component in TKE distribution is QF I and the high-energy one – QF II. Using this interpretation, the decomposition of TKE distribution for $E_{\mathrm{c.m.}}/E_{\mathrm{B}} = 1.00$ was done in [21]. To follow up the competition between QF I, QF II and CN fission in dependence on the interaction energy we have made the same analysis for all measured energies in this work. The lines in Figure 6 are the results of our decomposition. It is seen that the CN-fission component is found for all measured energies below as well as above the Coulomb barrier. The contribution of this component into all symmetric fissionlike fragments with masses $A\mathrm{CN}/2 \pm 20$ u formed in the reaction grows from 61% up to 72% when interaction energy increases from $E_{\mathrm{c.m.}}/E_{\mathrm{B}} = 0.95$ up to 1.04 and after decreases to 66% at $E_{\mathrm{c.m.}}/E_{\mathrm{B}} = 1.10$. It should be noted that for $^{48}\mathrm{Ca} + ^{238}\mathrm{U}$ the barrier for elongated collision is $E_{\mathrm{c.m.}}/E_{\mathrm{B}} = 0.90$ and for compact one is 1.02. Thus, the maximal CN-fission component is observed at energy close to the barrier for compact collisions.

Based on the assumption about the time distribution for QF process proposed in Ref. [34] together with the mass transfer equation from [3] it is possible to simulate the mass distribution for asymmetric QF fragments. The details of the simulation are given in [35].

The middle panel of Figure 6 shows the simulated mass spectra for QF I process together with estimated CN-fission components expected from LDM. The differences between the experimental distributions, QF I and CN fission correspond to QF II fragments (shown by the green lines in Figure 6). The QF I and CN-fission components were fitted in such a way that their contributions into the symmetric mass region were the same as the ones found from the TKE analysis described above.

The asymmetric component peaked at fragment masses of 131 and 155 u is clearly observed in experimental mass distributions at energy $E_{\mathrm{c.m.}}/E_{\mathrm{B}} = 1.00$. The yield of this asymmetric component is about 25%, which is twice higher than the estimated contribution of QF to the mass distribution. Recently, the mass and TKE distributions of fragments in the fission of even-even isotopes of superheavy elements from Hs ($Z = 108$) to Og ($Z = 118$) were estimated using a prescission point model [36]. The calculated mass yield for fission of ^{286}Cn at $E* = 30$ MeV is asymmetric with the light fragment peak near 134 u. Nevertheless, we expect the mass distribution of ^{286}Cn fission fragments to become close to Gaussian at higher CN excitation energies. The extracted components for QF II fragments are asymmetric at all interacting energies, the light peak is located around 110–116 u. No proton or neutron shells are predicted for these fragment masses.

While the estimated yield of CN fission component is more than 60% for sym-

metric reaction fragments for all studied energies, its contribution into all fission-like fragments is less than 15% at $E_{\mathrm{c.m.}}/E_{\mathrm{B}} = 1.10$ and drops down with decreasing interaction energy. The major part of all fissionlike events originates in QF I process at energies below and above the Coulomb barrier.

The maximal experimentally measured ER cross section is about 3 pb at energy close to the barrier of compact collisions [23]. Only the $3n$ and $4n$ evaporation channels were observed in the $^{48}\mathrm{Ca} + ^{238}\mathrm{U}$ reaction. For the lower energies no ER was found. One should note that all of the events observed in the production of isotopes of elements 112 and 114 with the fusion reactions $^{238}\mathrm{U}$, $^{242,244}\mathrm{Pu} + ^{48}\mathrm{Ca}$ were detected at energies above the Coulomb barrier, contrary to cold fusion reactions where the maximal yield of evaporation residues is observed at subbarrier energies [37].

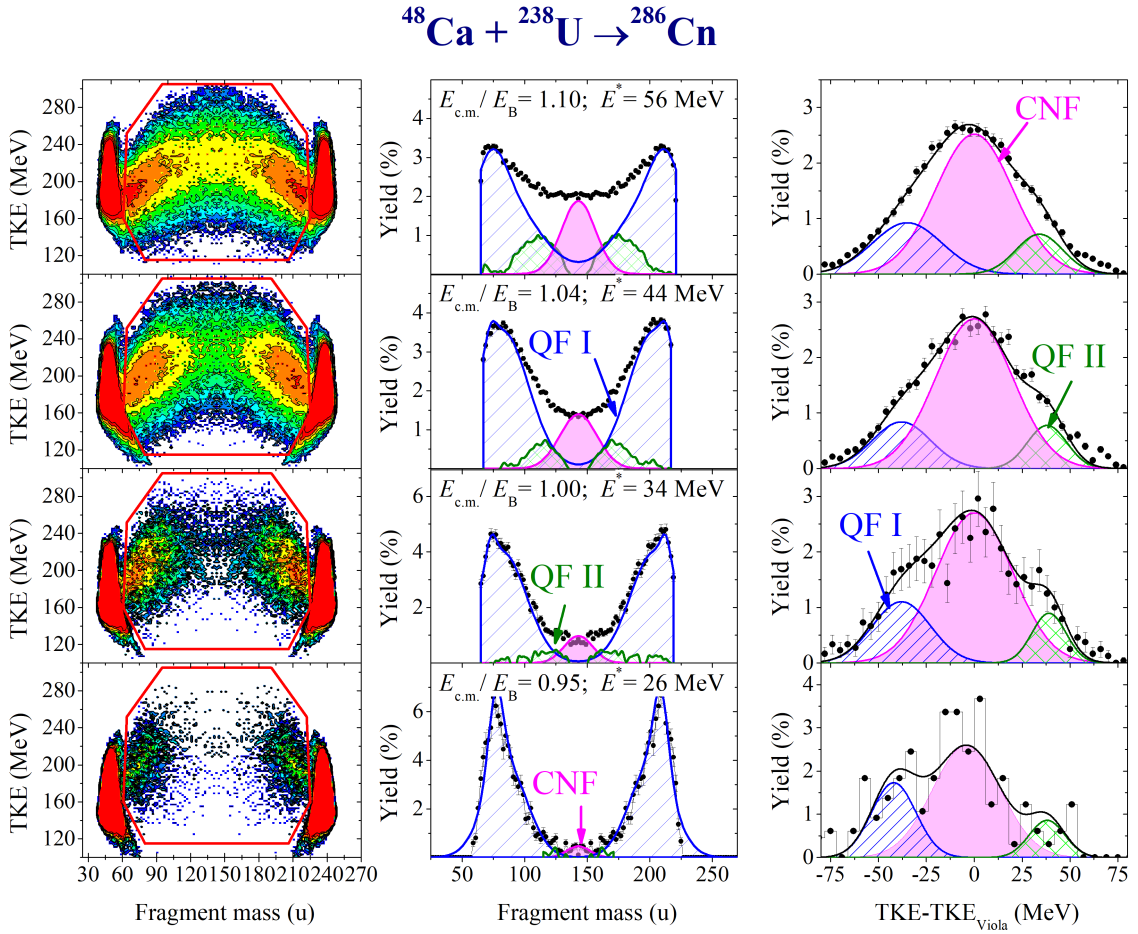

Figure 6: Left panel: Mass-energy distributions of binary fragments formed in the $^{48}\mathrm{Ca} + ^{238}\mathrm{U}$ reaction at energies near the Coulomb barrier from [21]. Red contours indicate the fission-like fragments. Middle panel: the experimental mass distributions for fission like fragments located inside the red contours in mass-energy distributions. The blue and green lines are the estimated contributions for QF I and QF II fragments, respectively, filled regions are the estimated yields for CN-fission process. Right panel: the experimental TKE distributions for symmetric fission-like fragments in the mass region 123–163 u and their decompositions into QF I, QF II (blue and green lines) and CN-fission (filled region) components.

Conclusions

The presence of orientation effects is found in mass-energy distributions of fissionlike fragments formed in the reactions of Ca ions with well deformed lanthanide nuclei as well as with actinides. It leads to increase of the yield of QF I at energies below the Coulomb barrier for both reaction types. The fragments originated in QF are localized near the closed proton and neutron shells, namely, the shells at $Z = 28$ and $N = 82$ for lanthanides, and at $Z = 28$, 82 and $N = 126$ for actinides play a key role. In the case of lanthanide targets, the QF I contribution into the capture cross section is about 20% at energies near the Coulomb barrier, and the main reaction mechanism is the CN formation. For actinide ones, QF I dominates (more than 95 %).

In the case of QF caused by elongated configuration at the reaction contact point the barrier distribution is shifted to lower energies with respect to the Coulomb barrier. The usage of the polarized actinide targets may possibly increase the fusion probability. According to our estimation, one may expect about one order of magnitude larger cross section of CN and QF II processes in the reactions leading to the formation of superheavy nuclei due to excluding the elongated configuration of interacting nuclei at contact point. Taking into account that for Ca-induced reactions with actinides the CN fission is the main process, whereas QF II is only 10-20%, the CN-formation cross section is expected to be several times larger in this case compared to not polarized actinide nuclei. Unfortunately, the preparing of polarized actinide targets is a difficult task not solved yet. Nevertheless, usage of polarized actinide targets can significantly increase the cross sections of SHN formation in the reactions with ions heavier than Ca.

References

[1] Yu. Ts. Oganessian and V. K. Utyonkov, Nucl. Phys. A **944**, 62 (2015).

[2] J. Toke *et al.*, Nucl. Phys. A **440**, 327 (1985).

[3] W. Q. Shen *et al.*, Phys. Rev. C **36**, 115 (1987).

[4] M. G. Itkis *et al.*, Nucl. Phys. A **944**, 204 (2015).

[5] E. Vardaci *et al.*, J. Phys. G: Nucl. Part. Phys. **46**, 103002 (2019).

[6] D. J. Hinde, M. Dasgupta, E. C. Simpson, Prog. Part. Nucl. Phys. **118**, 103856 (2021).

[7] M. G. Itkis *et al.*, Eur. Phys. J. A **58**, 178 (2022).

[8] V. V. Volkov, Phys. Rep. **44**, 93 (1978).

[9] G. G. Adamian, N. V. Antonenko, and W. Scheid, *Clusters in Nuclei, Vol. 2, Lect. Notes Phys.* **848**, 165 (2012).

[10] E. M. Kozulin *et al.*, Phys. Rev. C **86**, 044611 (2012).

[11] W. J. Swiatecki, Phys. Scr. **24**, 113 (1981).

[12] H. Abe, KEK Preprint 8-26, KEK TH-128, (1986).

[13] R. Du Rietz *et al.*, Phys. Rev. Lett. **106**, 052701 (2011).

[14] R. Smolańczuk, J. Skalski, and A. Sobiczewski, Phys. Rev. C **52**, 1871 (1995).

[15] P. Möller *et al.*, Phys. Rev. C **79**, 064304 (2009).

[16] M. Kowal, P. Jachimowicz, and A. Sobiczewski, Phys. Rev. C **82**, 014303 (2010).

[17] P. Jachimowicz, M. Kowal, and J. Skalski, Phys. Rev. C **95**, 014303 (2017).

[18] D. J. Hinde *et al.*, Phys. Rev. C **53**, 1290 (1996).

[19] G. N. Knyazheva *et al.*, Phys. Rev. C **75**, 064602 (2007).

[20] V. I. Zagrebaev, In: *Proc. of the 6th International Conference on Dynamical Aspects of Nuclear Fission (DANF 2006)*, World Scientific, Singapore, 2008, p.94.

[21] E. M. Kozulin *et al.*, Phys. Lett. B **686**, 227 (2010).

[22] A. M. Stefanini *et al.*, Eur. Phys. A **23**, 473 (2005).

[23] Yu. Ts. Oganessian *et al.*, Phys. Rev. C **70** (2004).

[24] A. Yu. Chizhov *et al.*, Phys. Rev. C **67**, 011603(R) (2003).

[25] E. M. Kozulin *et al.*, Instrum. Exp. Tech. **51**, 44 (2008).

[26] R. Vandebosch and J. R. Huizenga, *Nuclear Fission* (Academic, New York, 1973).

[27] N. Rowley, N. Grar, and M. Trotta, Phys. Rev. C **76**, 044612 (2007).

[28] V. Zagrebaev and W. Greiner, J. Phys. G: Nucl. Part. Phys. **31**, 825 (2005).

[29] V. Zagrebaev and W. Greiner, *Clusters in Nuclei, Vol. 1, Lect. Notes Phys.* **818**, 267 (2010).

[30] E. M. Kozulin *et al.*, Phys. Rev. C **94**, 054613 (2016).

[31] M. G. Itkis *et al.*, Nucl. Phys. A **734**, 136 (2004).

[32] A. Wakhle *et al.*, Phys. Rev. Lett. **113**, 182502 (2014).

[33] K. Nishio *et al.*, Phys. Rev. C **86**, 034608 (2012).

[34] R. Du Rietz *et al.*, Phys. Rev. Lett. **106**, 052701 (2011).

[35] G. N. Knyazheva *et al.*, Eur. Phys. J. Web of Conf. **63**, 02010 (2013).

[36] N. Carjan, F. A. Ivanyuk, and Yu. Ts. Oganessian, Phys. Rev. C **99**, 064606 (2019).

[37] G. Munzenberg, Nucl. Phys. A **944**, 5 (2015).